


Article

Effect of Surface Micro-Hardness Change in Multistep Machining on Friction and Wear Characteristics of Titanium Alloy

Guanming Hou ^{1,2} and Anhai Li ^{1,2,*} 

¹ Key Laboratory of High Efficiency and Clean Mechanical Manufacture of MOE, School of Mechanical Engineering, Shandong University, Jinan 250061, China; liahsea@163.com

² National Demonstration Center for Experimental Mechanical Engineering Education, Shandong University, Jinan 250061, China

* Correspondence: anhaili@sdu.edu.cn

Featured Application: High-efficiency machining of titanium alloy components for high wear resistance applications.

Abstract: The machined surface quality, especially the micro-hardness of machined surface layers, is strongly correlated to the friction and wear characteristics of titanium alloy engineering parts. Therefore, to explore relationship of the local surface micro-hardness change in multistep machining and the surface wear resistance of the machined parts is urgently necessary. The machined surfaces were acquired through two-step (roughing and finishing) and three step (roughing, semi-finishing, and finishing) cylindrical turning experiments. The dry friction and wear tests were carried out by UMT-2 friction and wear tester on the multistep final machined surface along the feed direction. The surface wear microtopography and subsurface microstructure were observed and analyzed by scanning electron microscope. The micro-hardness variation in the local area of the finishing surface will cause the extension of unstable friction time stage while withstanding the cyclic and alternating contact stresses, and the soft-hard alternating area should be the sources of friction and wear defects, for instance cracks, peeling pits, fracture striations and even the wear fracture zone to crack propagation and peeling off. This will be of great significance to accurately control the machined surface quality and adaptively improve the surface wear resistance of titanium alloy components.



Citation: Hou, G.; Li, A. Effect of Surface Micro-Hardness Change in Multistep Machining on Friction and Wear Characteristics of Titanium Alloy. *Appl. Sci.* **2021**, *11*, 7471. <https://doi.org/10.3390/app11167471>

Academic Editor: Pedro Rosa

Received: 14 July 2021

Accepted: 13 August 2021

Published: 14 August 2021

Publisher's Note: MDPI stays neutral with regard to jurisdictional claims in published maps and institutional affiliations.



Copyright: © 2021 by the authors. Licensee MDPI, Basel, Switzerland. This article is an open access article distributed under the terms and conditions of the Creative Commons Attribution (CC BY) license (<https://creativecommons.org/licenses/by/4.0/>).

Keywords: multistep machining; micro-hardness; standard deviation; friction and wear

1. Introduction

Titanium alloys are widely used in aerospace and navigation due to their high strength, low density and good corrosion resistance. However, due to the poor wear resistance of titanium alloys [1,2], their performance is seriously affected, which limits their application in this field. Friction and wear are common phenomena in the service use of mechanical parts. According to relevant statistical analysis [3], friction and wear occupied about 1/3 to 1/2 of the energy consumed by the equipment, and about 80% of the failure of machine parts is caused by friction and wear. Therefore, it is important to study and understand the influence of surface integrity on the friction and wear properties of titanium alloys, and to improve its performance and life.

Regarding the study of friction and wear properties, many scholars at home and abroad have devoted effort to the study of surface pretreatment (microelement coating, heat treatment of materials) or different experimental conditions. Cong et al. [4] found that the wear resistance of alloy samples (Low-carbon steel) at room temperature and 450 °C could be improved to some extent by performing double-glow plasma surface alloying treatment. The results showed that the alloy samples suffered mainly oxidative

wear at room temperature, and the main mechanisms of damage at high temperature were oxidative wear and fatigue delamination. Yao et al. [5] found that plating Cu on the surface of titanium alloy could significantly improve the surface wear resistance, and the wear resistance of the Cu coating layer was obviously superior to that of the titanium alloy matrix. The wear scar of the titanium alloy matrix was furrow morphology, and the wear mechanism was stripping wear and adhesive wear; the wear mechanism of the Cu coating layer was stripping wear and fatigue abrasion. By changing the experimental environment temperature, Yao et al. [6] studied the effect of the temperature on the friction and wear of the titanium alloys, and it was found that the surface was not oxidized at a low temperature, but at a higher temperature, there was significant oxidation on the wear scar surface, and oxidative wear occurred on the surface. Li et al. [7] performed the friction and wear of titanium alloy Ti-6Al-4V under dry sliding conditions by pin disc wear tester. It was found that the appearance and disappearance of surface friction oxides would change the friction and wear properties and even the wear mechanism of titanium alloys due to the change of sliding speed. Under the experimental conditions, stripping wear and oxidative wear would occur at low speeds, while at high speeds, there was only oxidative wear.

In order to improve the wear resistance, not only could the material be pretreated, but the cutting parameters and cutting process could also be optimized. Huang et al. [8] used a ball-end milling cutter to explore the influence of the tool milling path on the friction and wear of the die steel AISI D2. It was found that the ability of the material to resist friction and wear was closely related to the tool milling path. Due to the change of tool milling path, the degree of softening in near surface layer was the most obvious factor that affected friction and wear performance. The degree of softening determined the material spalling method and the severity of the plastic deformation, as well as the wear mechanism of the material.

Tang et al. [9] studied the wear behavior and mechanism of hardened die steel AISI D2 under different sliding speed and hardness level by dry sliding conditions. It was found that the wear loss was very sensitive to sliding speed and hardness. At the same time, due to the influence of hardness difference, different wear mechanisms were proposed. The main wear mechanism was adhesive wear under low hardness conditions and delamination wear under high hardness (referring to relative hardness). Yasavol et al. [10] and Singh et al. [11] found through experiments that the subsurface microstructure was refined and evenly twisted along the cutting direction, which could improve the surface friction and wear properties of the material.

The parts were usually obtained by a variety of machining methods and subjected to friction and wear during using. Especially for the advanced equipment, the performance and accuracy would be affected. Therefore, it was important to improve the friction and wear resistance. However, the effect of the machined surface obtained by multistep machining on the friction and wear properties of titanium alloys needed to be further revealed. Therefore, this paper aimed to study the effect of surface micro-hardness change (indicated by standard deviation) in multistep machining on the friction and wear characteristics along the feed direction. This will be of great significance to provide the basis for accurately controlling the high efficiency machined surface quality and adaptively improving the surface wear resistance of titanium alloy components for high wear resistance applications.

2. Cutting Materials and Experimental Preparation

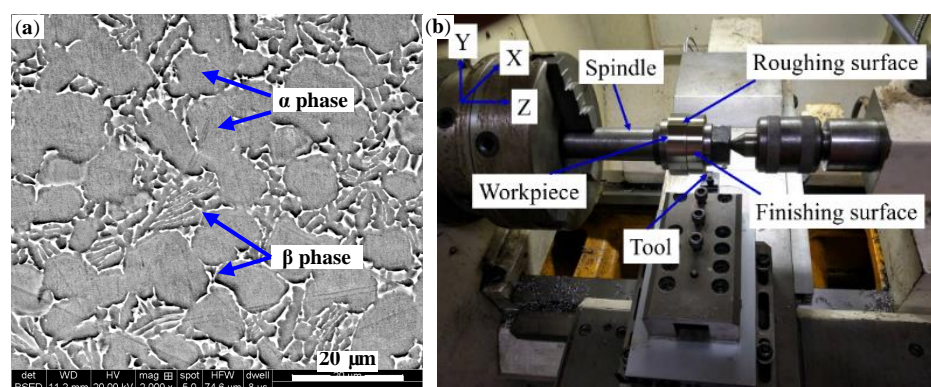
The titanium alloy Ti-6Al-4V was used as the experimental material, and the chemical composition and mechanical properties of titanium alloy are shown in Tables 1 and 2, respectively. The microstructure of Ti-6Al-4V alloy is exhibited in Figure 1, and the grey equiaxed α -Ti phase (hcp) and white β -Ti phase (fcc) shown in Figure 1a composes the $\alpha + \beta$ two-phase titanium alloy. The titanium alloy workpiece used in turning experiments was a bar dimension of $\varnothing 100 \text{ mm} \times 25 \text{ mm}$.

Table 1. Chemical composition of titanium alloy Ti-6Al-4V.

Element	Ti	Al	V	Fe	C	N	H	O	Other
Weight (wt.%)	base	5.5–6.75	3.6–4.5	0.3	0.08	0.05	0.15	0.10	0.50

Table 2. Mechanical and physical properties of titanium alloy at room temperature.

Density (kg/m ³)	Melting Point (°C)	Specific Heat at 25 °C (J/kg·°C)	Thermal Conductivity (W/m·K)	Yield Stress (MPa)	Young's Modulus (GPa)	Poisson's Ratio	Elongation (%)
4428	1605	580	7.3	825	110	0.41	10

**Figure 1.** Workpiece material and experimental setups. (a) Microstructure of Titanium alloy. (b) The cutting experiment equipment.

The experiments were conducted on a CKD6150H turning lathe under dry cutting conditions, and the experimental setup is shown in Figure 1b. A MSBNR2525M12 tool holder and the TiAlN-coated ultrafine grain WC-Co cemented carbide tools made by Zhuzhou Cemented Carbide Cutting Tools Co., Ltd., Zhuzhou, China was used in the multistep turning experiments. The type of roughing tool was SNMG120408-EF, and the type of semi-finishing and finishing tools were both SNMG120404-EM. The two kinds of tool inserts are both square shaped inserts with a TiAlN coating (type YBG202), double-side chip breaking groove, a 12.7 mm length and width, and a thickness of 4.76 mm. The corner radii of SNMG120408-EF insert and SNMG120404-EM insert are 0.8 mm and 0.4 mm, respectively. The YBG202 type TiAlN coating is combined with the high strength and toughness tool substrate of ultrafine grain WC-Co carbide, which is suitable for finish and semi-finish turning of all kinds of processed materials and rough turning of superalloys. After the tool was installed in the tool holder, the working rake angle was 14° and the clearance angle was 11°.

The final machined surface was obtained by two-step machining (firstly roughing, and finally finishing) and three-step machining (firstly roughing, then semi-finishing, and finally finishing). In the two-step machining, the roughing cutting parameters were variable, as shown in Table 3, the finishing cutting parameters were fixed, the machining was conducted at the cutting speed of 100 m/min, feed rate of 0.05 mm/r, and depth of cut of 0.1 mm. In the three-step machining, the cutting parameters were all fixed, and the roughing machining was carried out at the cutting speed of 50 m/min, feed rate of 0.25 mm/r, and depth of cut of 1.0 mm, the semi-finishing cutting parameters were set at the cutting speed of 80 m/min, feed rate of 0.15 mm/r, and depth of cut of 0.3 mm. In the three-step machining, the finishing cutting parameters were the same as those in the two-step machining. The experimental trials under all cutting conditions were repeated and verified on the condition that fluent chip breaking effect and stable chip formation process was acquired. At the same time, in order to reduce the influence of tool wear on the machining, a new tool would be used each time the machining was performed.

Table 3. Roughing cutting parameters and cutting conditions for the experimental work.

Cutting Tool	SNMG120408-EF and SNMG120404-EM
Cutting speed, v (m/min)	30, 50, 70
Depth of cut, a_p (mm)	0.5, 1.0, 1.5
Feed rate, f (mm/r)	0.25
Tool geometry	rake angle 14° and clearance angle 11°

Using the HVS-1000 Vickers micro-hardness instrument, the micro-hardness at $100\ \mu\text{m}$ below the surface after roughing and the finishing surface micro-hardness was measured along the feed direction. Figure 2 was a schematic diagram describing the change of micro-hardness in the local area of surface layer. Among them, $abcd$ was roughing surface, ef was circumferential curve, and hg was roughing tool path curve. Meanwhile, $ABCD$ was the obtained finishing surface when the depth of cut a_p was $0.1\ \text{mm}$, EF was circumferential curve, and HG was finishing tool path curve. The micro-hardness measurement results showed that there was a difference in the micro-hardness of the local area along the feed direction after roughing. For example, there was a difference in the micro-hardness at points i and j . Since gh was the tool path curve, the micro-hardness was the same at points j and k in theory, and ef was the circumferential curve. Therefore, there was a difference in the micro-hardness at points i and k . Additionally, in addition to the tool path curve, there was a difference for micro-hardness in the local area of machined surface. By measuring the micro-hardness at $100\ \mu\text{m}$ below the surface after roughing along the feed direction, it was found that the difference existed not only in the surface but also in the range of the depth Δl . Because the finishing depth of cut a_p was $0.1\ \text{mm}$, within the range of the roughing micro-hardness affected layer depth Δl . Therefore, the surface layer micro-hardness after roughing would affect the finishing machining, and affecting the finishing surface micro-hardness, thus affecting the friction and wear characteristics of the titanium alloy.

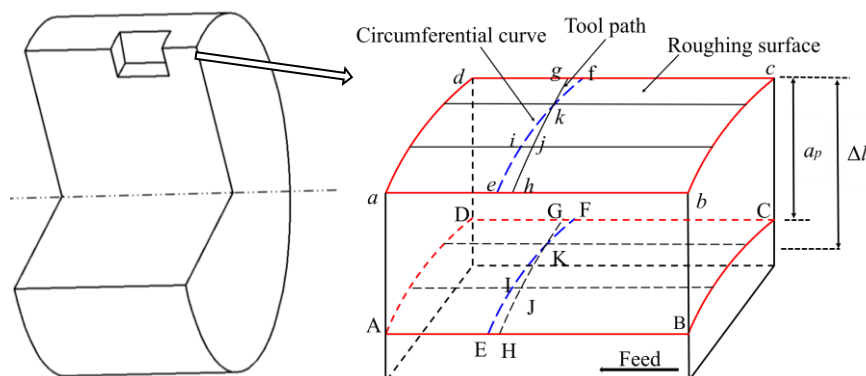
**Figure 2.** Schematic diagram of surface layer micro-hardness analysis.

Figure 3 were schematic diagrams of the roughing surface layer micro-hardness and the finishing surface micro-hardness, respectively. Five points (Marked as point 1, point 2, point 3, point 4, and point 5, respectively) were measured in the unit feed (The length of unit feed was $250\ \mu\text{m}$, which is the roughing feed rate). When measuring, the first measurement point could be freely selected, and then each point was measured every $50\ \mu\text{m}$ in turn. Additionally, the total length was measured to be $1250\ \mu\text{m}$ (5 times the roughing feed rate). When measuring, the applied load was $100\ \text{g}$ and the loading time was $15\ \text{s}$.

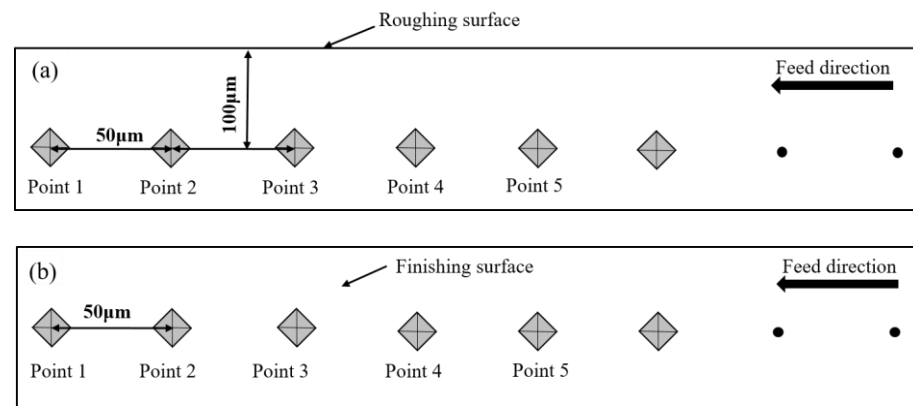


Figure 3. The schematic diagrams of the micro-hardness measurement along the feed direction. (a) Roughing micro-hardness at the depth of 100 μm below the machined surface (cross section). (b) The finishing surface micro-hardness (top view).

In the friction process, the friction tests were carried out using a UMT-2 friction tester, and the reciprocating test of the ball disc contact was adopted. Figure 4 was a schematic diagram of friction and wear, and Figure 4a was the experiment equipment. For the convenience of the experiment, the finishing surface was subjected to wire cutting, and Figure 4b was a wire-cut sample to be rubbed. Additionally, Figure 4c was a front view and Figure 4d was a left side view. The experiment was carried out at room temperature, and the pair of grinding balls were bearing steel (GCr15, hardness was 36–40 HRC), and the hardness was higher than that of titanium alloy. The load applied on the contact surface was 5 N, the reciprocating sliding speed was 8 mm/s, the sliding distance was 4 mm, and the friction time was 15 min or 30 min, respectively. Finally, the surface wear microtopography and subsurface microstructure were observed by scanning electron microscope. Considering that the width of the wear band is relatively small, less than 1 mm, when observing the worn surface layer, the observation was made along the cutting direction.

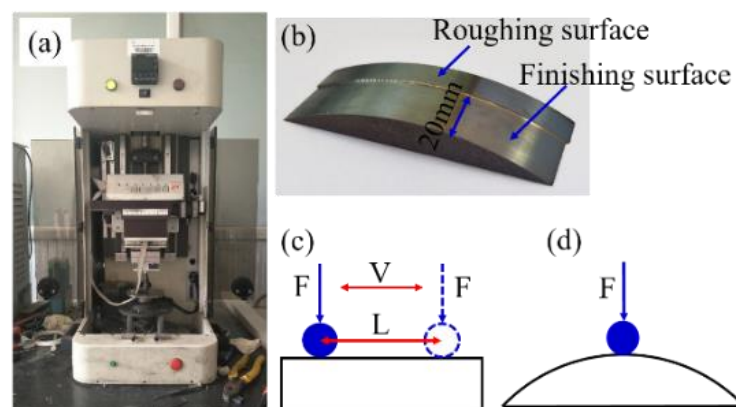


Figure 4. The schematic diagrams of friction and wear. (a) Experiment equipment. (b) The wire-cut sample to be rubbed. (c) Front view. (d) Left side view.

3. Experimental Results and Analysis

Based on many scholars' researches on the cutting process, the temperature and stress gradients in local areas during the formation of the machined surface layer has been investigated by finite element simulation. The cutting forces cause stress gradients in local areas instantaneously [12–14] during cutting, and the temperature at the contact area between the tool tip and the machined surface would be different [15–18]. On this basis, the unit feed periodic machining was proposed. It was considered that in the ideal state, along the feed direction, the cutting force (the magnitude and direction of force were same)

and the cutting temperature were the same at the corresponding point, for example, points A and B in Figure 5a. The cutting force and temperature were different near the adjacent points in the unit feed, as shown by the curve *abc* in Figure 5a. At the same time, the surface integrity also showed periodic changes along the feed direction. For example, the surface topography showed a certain regular peak and valley, and the valley was a path on which the tool passed in the cutting direction, as shown in Figure 5b. The differences of cutting force and temperature in the unit feed resulted in the differences of micro-hardness in local areas.

Normally, the unit feed periodic machining did not take into account the factors such as tool wear and cutting vibration during the cutting process. These factors caused the periodicity of surface integrity to change along the feed direction. To minimize the effects of tool wear, the new tools were replaced before next machining. At the same time, in order to improve the roundness, each sample was subjected to multipass to reduce the cutting vibration before the experiment. Because the degree of work hardening of the vibrating turning [19] was higher than that of ordinary turning, and the difference of surface layer micro-hardness in the local area would cause the turning vibration in the ordinary turning process, which in turn caused a significant change in the finishing surface micro-hardness of the localized area.

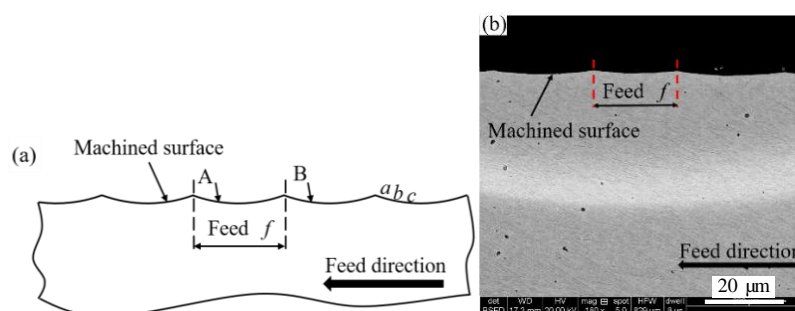


Figure 5. Cross-sectional schematic diagrams of the unit feed periodic machining along the feed direction. (a) Cross-sectional schematic diagram in ideal machining conditions. (b) Cross-sectional schematic diagram in actual machining conditions.

In this paper, the effect of roughing surface layer micro-hardness on the finishing surface micro-hardness was studied. Additionally, then the effect of finishing surface micro-hardness change on the friction and wear properties of titanium alloy were investigated along the feed direction.

3.1. Micro-Hardness

In the high-speed machining process, the micro-hardness changed significantly within a certain depth of the surface layer due to the cutting force, cutting temperature, the extrusion and friction of the tool and the workpiece surface. This was especially true the subsurface, which was softened due to poor thermal conductivity, and the surface layer within a certain depth was subjected to work hardening due to the influence of the cutting force [20]. In this experiment, roughing micro-hardness at the depth of 100 μm below the machined surface and the finishing surface micro-hardness were measured along the feed direction, respectively.

Figure 6 showed the variation curve of roughing surface layer micro-hardness in the unit feed, Figure 7 showed the variation curve of finishing surface micro-hardness in the unit feed. According to the micro-hardness value of each measurement point, Figure 8 was the standard deviation of the roughing surface layer micro-hardness and the finishing surface micro-hardness. It could be seen from Figures 6 and 7 that the micro-hardness value of the roughing surface layer or the finishing surface in the unit feed did not show a significant change along the feed direction.

Due to the poor thermal conductivity of titanium alloy, the cutting heat generated during the cutting process only acted on the contact area of the tool-chip-part, and the influence on surface layer was not too deep [21]. So, the micro-hardness was not much affected by the cutting heat, and it was more affected by the cutting force during machining. It can be seen from Figures 6 and 8 that the larger the roughing cutting speed or depth of cut was, the more greatly the roughing surface layer micro-hardness in the unit feed fluctuated along the average micro-hardness value, and the standard deviation was larger. This was mainly because, during the roughing process, the larger the cutting speed or depth of cut was, the higher the cutting force and temperature were, the greater the gradients changed in unit feed (especially the stress gradients), the greater the micro-hardness changed along the feed direction. At the same time, different degrees of tool flank wear affected by cutting force and temperature caused also uneven stress in the cutting area, which in turn led to the difference of surface layer micro-hardness in the local area.

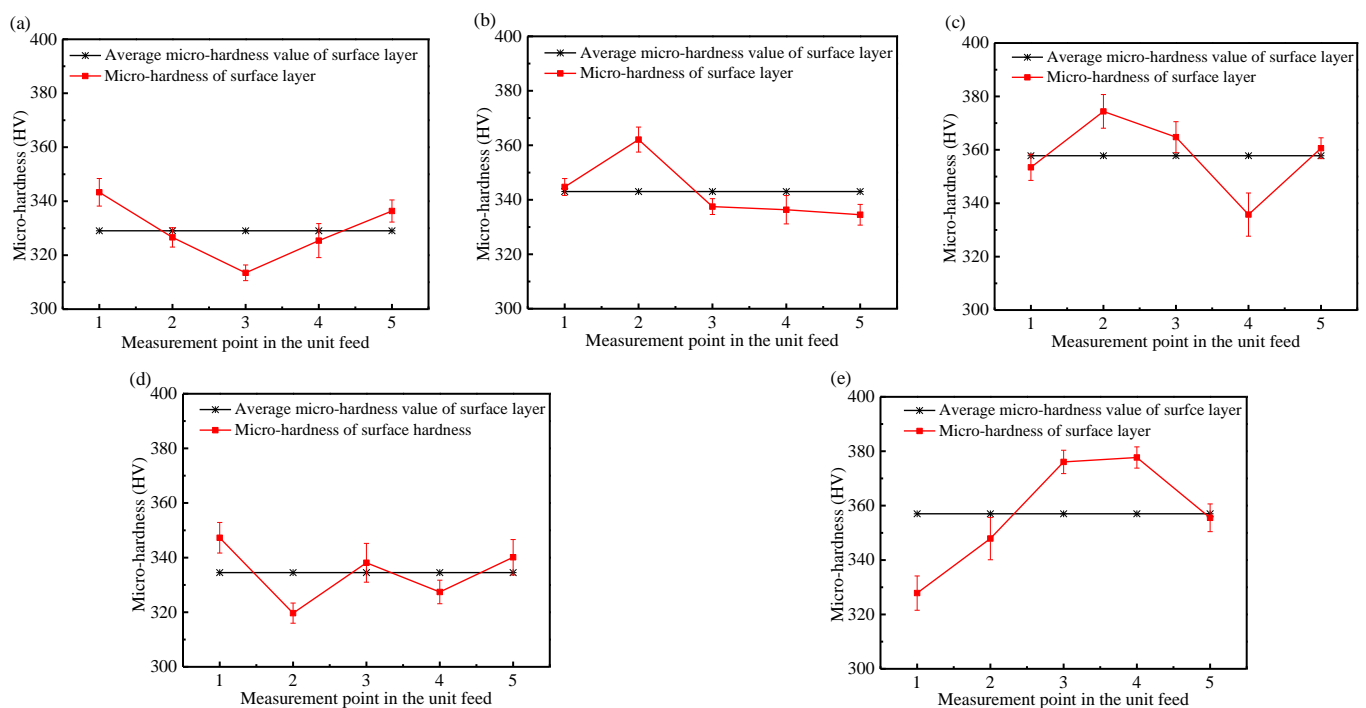


Figure 6. The roughing surface layer micro-hardness in the unit feed. (a) $v = 30$ m/min, $f = 0.25$ mm/r, $a_p = 1.0$ mm. (b) $v = 50$ m/min, $f = 0.25$ mm/r, $a_p = 1.0$ mm. (c) $v = 70$ m/min, $f = 0.25$ mm/r, $a_p = 1.0$ mm. (d) $v = 50$ m/min, $f = 0.25$ mm/r, $a_p = 0.5$ mm. (e) $v = 50$ m/min, $f = 0.25$ mm/r, $a_p = 1.5$ mm.

As could be seen from Figure 7a–e, when the roughing cutting speed v was 70 m/min or depth of cut a_p was 1.5 mm, the finishing surface micro-hardness in the unit feed fluctuated more greatly along the average micro-hardness value, and the standard deviation is larger. At the same time, it could be seen that when the roughing depth of the cut was 0.5 mm, the finishing surface micro-hardness in the unit feed had a relatively small fluctuation along the average micro-hardness value, and the standard deviation was relatively small. This was mainly because there was a difference in the surface layer micro-hardness after roughing, which caused the cutting vibration when finishing, in turn resulting in the fluctuations of the finishing surface micro-hardness in the unit feed. Additionally, the greater the difference of the roughing surface layer micro-hardness was, the greater the fluctuation of the finishing surface micro-hardness in the unit feed was, and the larger the standard deviation was.

Figure 7f was the finishing surface micro-hardness in the three-step machining. It could be seen that the finishing surface micro-hardness in the unit feed fluctuated little along the average micro-hardness value, and the standard deviation was 8.39, which was

significantly lower than the standard deviation in the two-step machining. This was mainly because during the three-step machining, semi-finishing reduced the influence of roughing on work hardening of the surface layer. Therefore, the difference of the surface layer micro-hardness was reduced when finishing, and the standard deviation was relatively small.

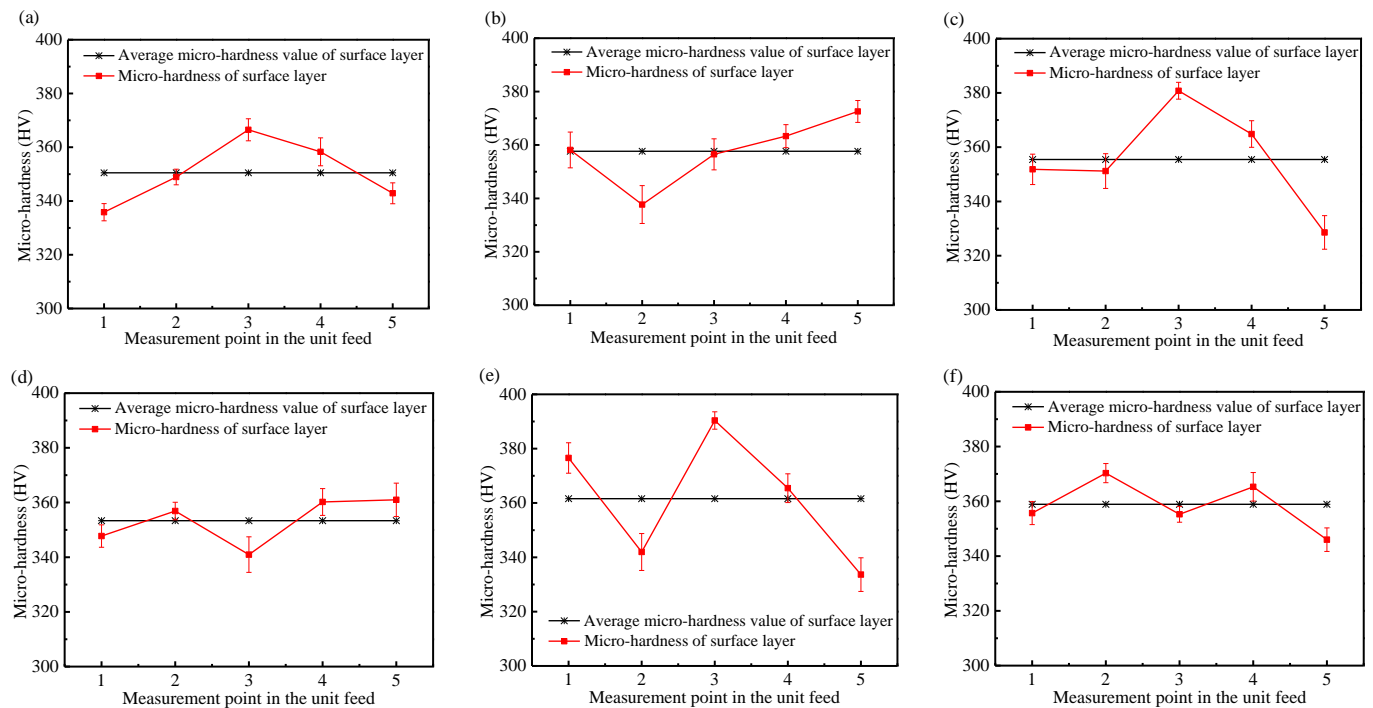


Figure 7. The finishing surface micro-hardness in the unit feed. (a) $v = 30$ m/min, $f = 0.25$ mm/r, $a_p = 1$ mm. (b) $v = 50$ m/min, $f = 0.25$ mm/r, $a_p = 1.0$ mm. (c) $v = 70$ m/min, $f = 0.25$ mm/r, $a_p = 1.0$ mm. (d) $v = 50$ m/min, $f = 0.25$ mm/r, $a_p = 0.5$ mm. (e) $v = 50$ m/min, $f = 0.25$ mm/r, $a_p = 1.5$ mm. (f) $v = 80$ m/min, $f = 0.15$ mm/r, $a_p = 0.3$ mm.

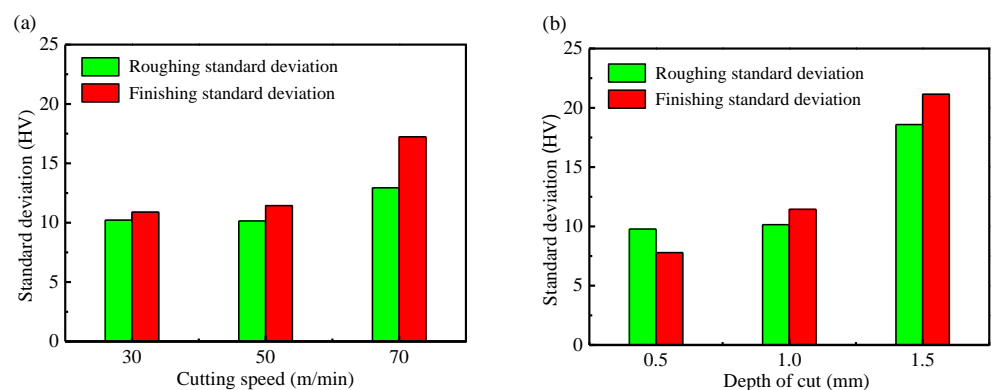


Figure 8. Effect of roughing cutting parameters on the standard deviation of roughing surface layer and finishing surface micro-hardness. (a) $f = 0.25$ mm/r, $a_p = 1.0$ mm. (b) $v = 50$ m/min, $f = 0.25$ mm/r.

3.2. Friction Coefficient Curve

According to the change of friction coefficient with time, this paper divided the friction coefficient curve into three parts: $0-t_1$ s, run-in friction phase; t_1 s– t_2 s, stable friction phase; after t_2 s, intense friction phase. In order to further study the friction and wear characteristics of titanium alloy machined surface, this paper focuses on the length of the stable friction phase, Δt , and $\Delta t = t_2 - t_1$. According to the Δt , the wear resistance of multistep machined surface was investigated.

Figure 9 shows the friction coefficient curve of machined surface as time under different cutting conditions. It can be seen from Figure 9 that the stable friction phase times Δt_a , Δt_b , Δt_d , and Δt_f show no apparent differences, and the stable friction phase time Δt was about 500 s. However, for Δt_c and Δt_e , the stable friction phase time Δt were significantly lower than 500 s, especially Δt_e , the stable friction phase time Δt was about 300 s. The main reason for the significant difference about the stable friction phase time Δt of the machined surface is that, due to the influence of the previous step (especially roughing), it could be found from Figure 8 that there was a difference in the machined surface micro-hardness of the localized area after finishing (indicated by standard deviation). The larger the standard deviation was, the greater the change of micro-hardness in the localized area of the machined surface, the greater the plasticity difference of the material, and the more easily the machined surface subjected to alternating contact stress was peeled off, making it that much easier to reach the intense friction phase, thereby leading to the shorter the frictional phase time Δt .

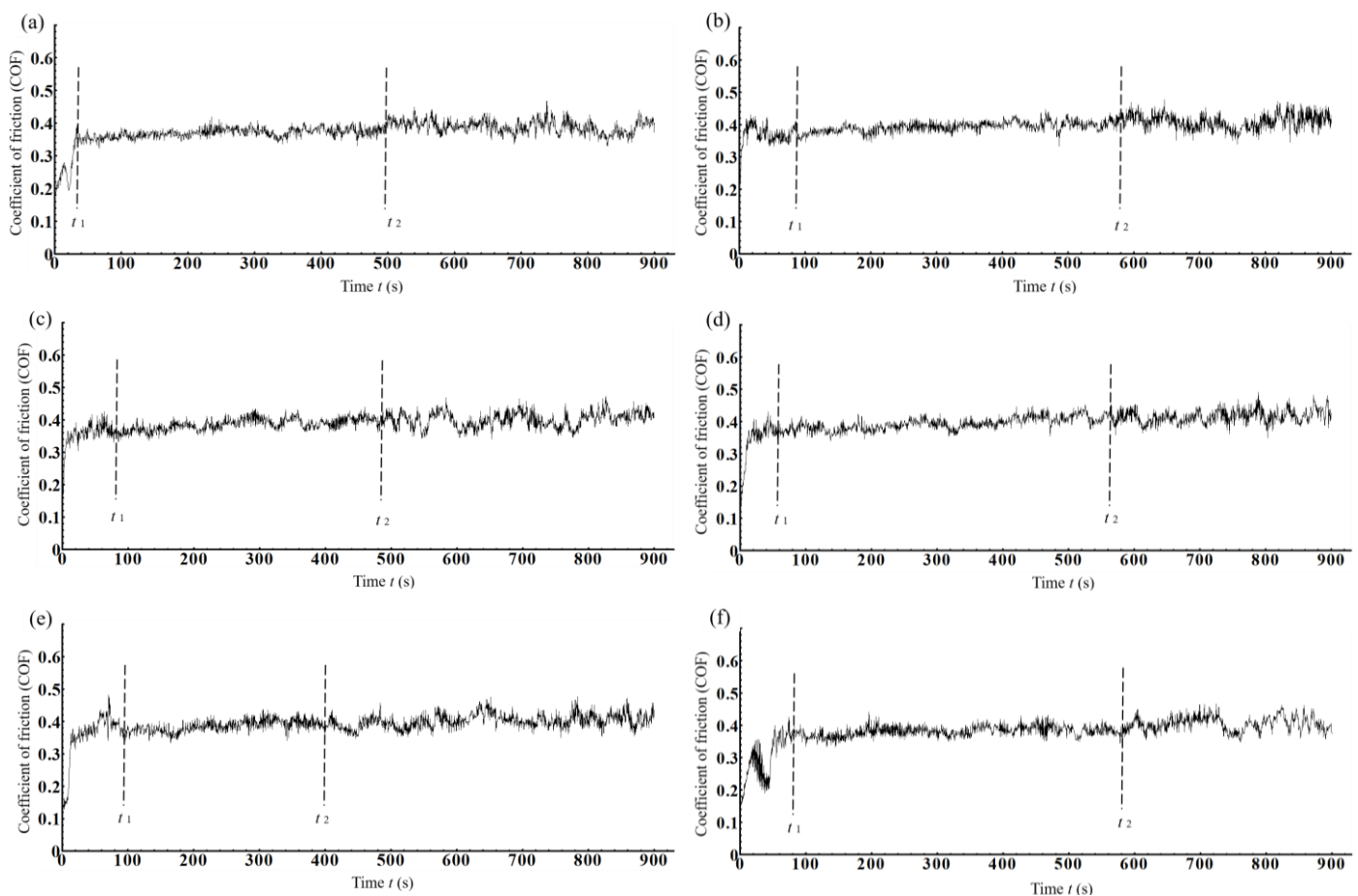


Figure 9. The friction coefficient curve of machined surface vs. time. (a) $v = 30$ m/min, $f = 0.25$ mm/r, $a_p = 1$ mm. (b) $v = 50$ m/min, $f = 0.25$ mm/r, $a_p = 1$ mm. (c) $v = 70$ m/min, $f = 0.25$ mm/r, $a_p = 1$ mm. (d) $v = 50$ m/min, $f = 0.25$ mm/r, $a_p = 0.5$ mm. (e) $v = 50$ m/min, $f = 0.25$ mm/r, $a_p = 1.5$ mm. (f) $v = 80$ m/min, $f = 0.15$ mm/r, $a_p = 0.3$ mm.

3.3. Surface Wear Microtopography

Figure 10 shows that the surface wear microtopography was observed after 15 min in the two-step machining. Figure 11a,b show the surface wear microtopography observed after 15 min and 30 min in the three-step machining, respectively. Additionally, Figure 12a,b show the wear loss measured after 15 min and 30 min in the two-step machining, respectively. It could be seen from Figures 10 and 12 that within the roughing cutting speed parameters, when the roughing cutting speed was 50 m/min, the surface wear spalling

area was relatively minimal and the wear loss was the least. On the contrary, when the roughing cutting speed was 70 m/min, the surface wear spalling area was the largest and the wear loss was the most. As the roughing depth of the cut increased, the surface wear spalling area was more severe and the wear loss was greater. It could be seen from Figure 11 that, as the friction time increased, the surface wear spalling area significantly enlarged, and the wear loss was more serious. When the cutting speed was 70 m/min or the cutting depth was 1.5 mm, it could be found from Figure 10a,b that severe spalling appeared on the surface by the amplification of local area, and wear fracture striations occurred due to spalling.

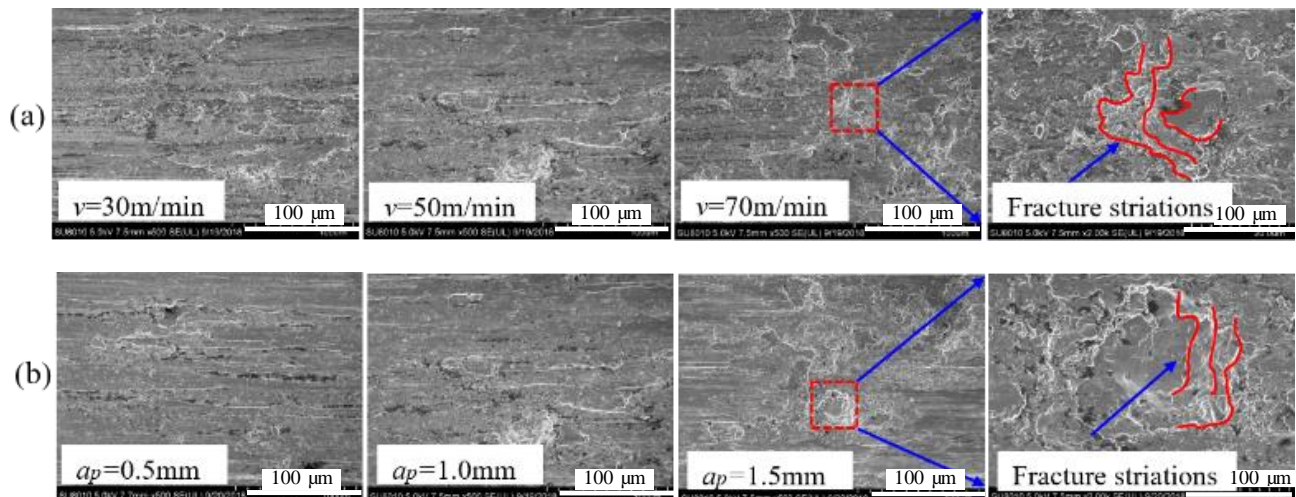


Figure 10. The surface wear microtopography observed after 15 min in the two-step cutting condition. (a) $f = 0.25$ mm/r, $a_p = 1$ mm. (b) $v = 50$ m/min, $f = 0.25$ mm/r.

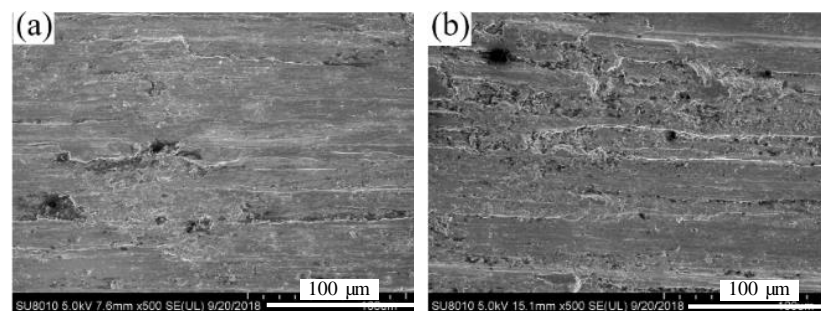


Figure 11. The surface wear microtopography under different friction times in the three-step machining. (Roughing cutting parameters: $v = 50$ m/min, $f = 0.25$ mm/r, and $a_p = 1.0$ mm; Semi-finishing cutting parameters: $v = 80$ m/min, $f = 0.15$ mm/r, and $a_p = 0.3$ mm). (a) 15 min. (b) 30 min.

Although the finishing cutting conditions and the process of the friction experiment were the same, the surface wear spalling and wear loss were significantly different. The main reason was that the change of roughing surface layer micro-hardness has an effect on the finishing surface micro-hardness to some extent [22], which led to differences in finishing surface micro-hardness in the local area. The greater the difference of micro-hardness in the local area was, the greater the difference of plastic deformation of the material was. The surface layer subjected to alternating contact stress was more prone to cracks during the friction process, which in turn peeled off. Therefore, the surface wear spalling was different, the wear loss was different. Additionally, the surface wear spalling and wear loss were positively correlated with the standard deviation of micro-hardness.

Figure 13 showed the subsurface wear microtopography under different friction times. It was found from Figure 13 that the cracks occurred in the subsurface layer, and even

spalling pits appeared. The longer the friction time was, the more severe the surface wear spalling area was. This was mainly because there was a change in the finishing surface micro-hardness in the unit feed along the feed direction. The greater the standard deviation was, the greater the difference of plastic deformation of the material was. At the same time, since the alternating contact stress during the friction process was quite high, cracks appeared in the weak area of surface layer. As the experiment progressed, the crack spread and peeled off, and even the spalling pits occurred due to cyclic impact spalling.

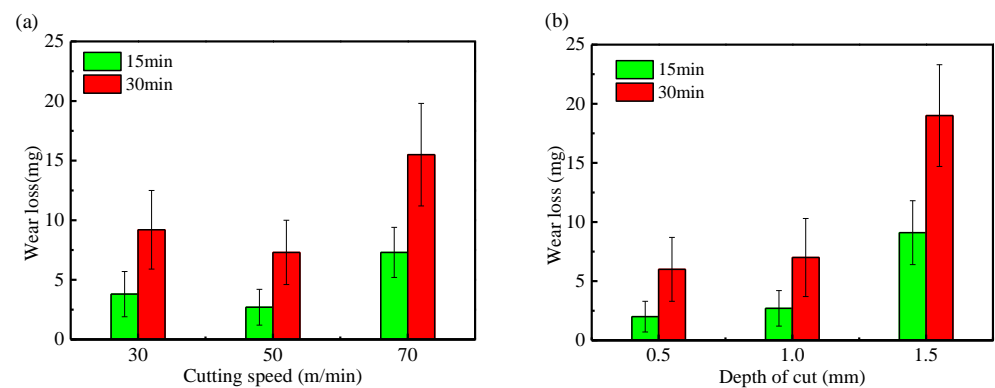


Figure 12. The effect of the change of roughing cutting parameters on wear loss of titanium alloy under different friction times. (a) $f = 0.25$ mm/r, $a_p = 1$ mm. (b) $v = 50$ m/min, $f = 0.25$ mm/r.

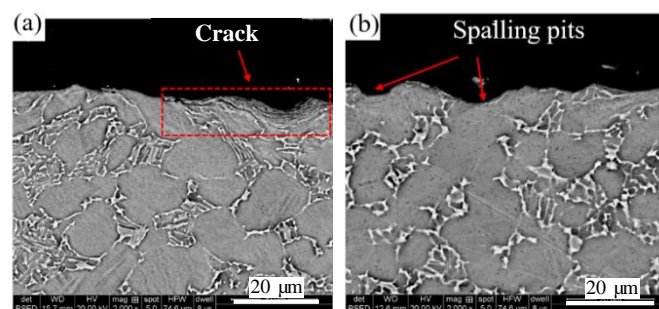


Figure 13. The subsurface wear microtopography under different friction times ($v = 50$ m/min, $f = 0.25$ mm/r, and $a_p = 0.5$ mm). (a) 15min. (b) 30 min.

3.4. Wear Mechanism Analysis

Hardness refers to the resistance of local area of the material to the hard object being pressed into its surface. It is an indicator of the degree of softness and hardness between various materials. Regarding the study of hardness on the friction properties of the material, generally speaking, the material with relatively high hardness had good wear resistance [23]. However, some studies had found that [9] the increase in hardness would make the deterioration of near-surface cracks more serious. This was mainly because the hardness increased, the material was more brittle, and the cracks and delamination wear were easily caused during friction, the wear resistance was worse and the wear rate was higher. At the same time, the hardness was lower, the plasticity was relatively larger, so the wear resistance was better. However, some studies had found that [24] reasonable improvement of the hardness of the core of the carburized steel could effectively improve the surface fatigue wear resistance. Because the carburized layer was too shallow, cracks would occur in the transition zone between the hardened layer and the core, causing the surface layer to peel off.

Figure 14 was a cross-sectional schematic diagram showing the difference of the finishing subsurface layer micro-hardness, and the force was applied to the local area of the finishing surface along the feed direction. The blue area A was a relatively hard area, and the red area B was a relatively soft area (The degree of softness and hardness was relative

to the average micro-hardness), and the broken line C was an easy spalling area in theory. During the experiment, the conditions applied in the adjacent regions were identical, so in the areas A and B, the horizontal component F_1 and the vertical component F_2 of the force F were the same, respectively. Due to the high hardness, the plasticity deformation of the area A subjected to the F_1 was relatively small along the feed direction, and on the contrary, the plasticity deformation was relatively large in the area B due to the low hardness. However, in the transition zone of A and B, the micro-hardness changed significantly, so the plasticity difference changed greatly. When subjected to the alternating contact stress during the friction process, it was easier to cause cracks under the cyclic reciprocating conditions. The crack expanded continuously and eventually peeled off to form a spalling pit, and even the wear fracture striations occurred due to spalling. Therefore, by selecting appropriate cutting steps and parameters, the standard deviation of micro-hardness could be reduced and the friction and wear resistance of titanium alloy could be improved.

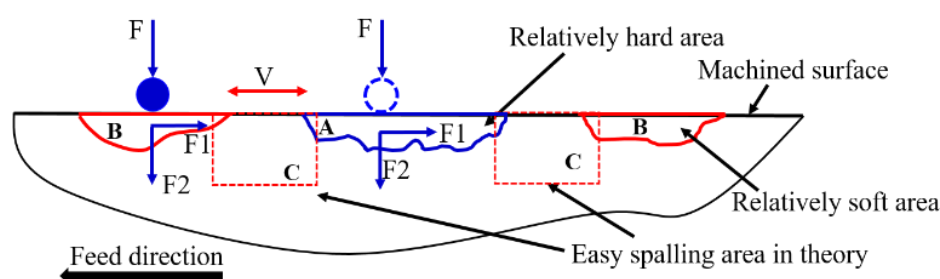


Figure 14. The cross-sectional schematic diagram of the difference of the surface layer micro-hardness in the local area along the feed direction.

4. Conclusions

Multistep cylindrical turning experiments of titanium alloy were performed to acquire the finishing machined surfaces. The friction and wear tests were carried out by UMT-2 friction and wear testing under dry sliding conditions along the feed direction. The effect of final finishing machined surface micro-hardness on the friction and wear properties of titanium alloy was studied. The main conclusions were as follows:

- (1) The local area of micro-hardness at 100 μm below the surface along the feed direction after roughing was obviously affected by the cutting parameters. In the multistep cutting process, affected by the roughing work hardening, the local area of the finishing surface micro-hardness will change versus the roughing cutting parameters. During the three-step machining, semi-finishing reduced the influence of roughing on work hardening of the surface layer, thereby reducing the local variation of finishing surface microhardness.
- (2) Through observing the surface wear microtopography and subsurface microstructure were observed and analyzed by scanning electron microscope, the micro-hardness variation in the local area of the finishing surface, mainly reflected by the change in standard deviation of micro-hardness measurement results along the feed direction, will cause the extension of unstable friction time stage while withstanding the cyclic and alternating contact stresses.
- (3) The soft-hard alternating area should be the sources of friction and wear defects, for instance cracks, peeling pits and even the wear fracture zone to crack propagation and peeling off. The friction and wear of the finishing surface was positively correlated with the local change of the machined surface micro-hardness. Adjusting and controlling the machined surface quality in multistep machining will thereby help to improve the friction and wear resistance of the finishing titanium alloy components.

Author Contributions: Conceptualization, G.H. and A.L.; methodology, G.H.; software, G.H.; validation, G.H. and A.L.; formal analysis, G.H.; investigation, G.H. and A.L.; data curation, G.H.; writing—original draft preparation, G.H.; writing—review and editing, G.H. and A.L.; visualization, G.H.; supervision, A.L.; project administration, A.L.; funding acquisition, A.L. All authors have read and agreed to the published version of the manuscript.

Funding: This research was funded by the National Natural Science Foundation of China (51605260), the Key Research and Development Program of Shandong Province (2019JZZY010114), and the Young Scholars Program of Shandong University (2018WLJH57).

Institutional Review Board Statement: Not applicable.

Informed Consent Statement: Not applicable.

Data Availability Statement: The datasets generated and analyzed during the current study are available from the corresponding author on reasonable request.

Conflicts of Interest: The authors declare no conflict of interest.

References

1. Rack, H.J.; Qazi, J.I. Titanium alloys for biomedical applications. *Mater. Sci. Eng. C* **2006**, *26*, 1269–1277. [\[CrossRef\]](#)
2. He, Z.Y.; Wang, Z.X.; Wang, W.B.; Fan, A.L.; Xu, Z. Surface modification of titanium alloy Ti6Al4V by plasma niobium alloying process. *Surf. Coat. Technol.* **2007**, *201*, 5705–5709. [\[CrossRef\]](#)
3. Liu, Y.; Yang, D.Z.; He, S.Y.; Wu, W.L. Microstructure developed in the surface layer of Ti-6Al-4V alloy after sliding wear in vacuum. *Mater. Charact.* **2003**, *50*, 275–279. [\[CrossRef\]](#)
4. Cong, W.; Yao, Z.J.; Zhu, X.L. Sliding wear of low carbon steel modified by double-glow plasma surface alloying with nickel and chromium at various temperatures. *Wear* **2010**, *268*, 790–796. [\[CrossRef\]](#)
5. Yao, X.F.; Xie, F.Q.; Wang, Y.F.; Wu, X.Q. Study on friction and wear properties of titanium alloy by plating Cu on the surface. *Rare Met. Mater. Eng.* **2012**, *41*, 2135–2138.
6. Yao, X.F.; Xie, F.Q.; Han, Y.; Zhao, G.X.; Wu, X.Q. Effect of temperature on wear properties and friction coefficient of titanium alloy. *Rare Met. Mater. Eng.* **2012**, *41*, 1463–1466.
7. Li, X.X.; Zhou, Y.; Ji, X.L.; Li, Y.X.; Wang, S.Q. Effects of sliding velocity on tribo-oxides and wear behavior of Ti-6Al-4V alloy. *Tribol. Int.* **2015**, *91*, 228–234. [\[CrossRef\]](#)
8. Huang, W.M.; Zhao, J.; Ai, X.; Wang, G.J.; Zhong, X. Influence of tool path strategies on friction and wear behavior of high-speed ball-end-milled hardened AISI D2 steel. *Int. J. Adv. Manuf. Technol.* **2018**, *96*, 2769–2779. [\[CrossRef\]](#)
9. Tang, L.H.; Gao, C.X.; Huang, J.L.; Zhang, H.Y.; Chang, W.C. Dry sliding friction and wear behaviour of hardened AISI D2 tool steel with different hardness levels. *Tribol. Int.* **2013**, *66*, 165–173. [\[CrossRef\]](#)
10. Yasavol, N.; Ramalho, A. Wear properties of friction stir processed AISI D2 tool steel. *Tribol. Int.* **2015**, *91*, 177–183. [\[CrossRef\]](#)
11. Singh, K.; Khatirkar, R.K.; Sapate, S.G. Microstructure evolution and abrasive wear behavior of D2 steel. *Wear* **2015**, *328*, 206–216. [\[CrossRef\]](#)
12. Davoudinejad, A.; Tosello, G.; Parenti, P.; Annoni, M. 3D finite element simulation of micro end-milling by considering the effect of tool run-out. *Micromachines* **2017**, *8*, 187. [\[CrossRef\]](#)
13. Zang, J.; Zhao, J.; Li, A.H.; Pang, J.M. Serrated chip formation mechanism analysis for machining of titanium alloy ti-6al-4v based on thermal property. *Int. J. Adv. Manuf. Technol.* **2018**, *98*, 119–127. [\[CrossRef\]](#)
14. He, L.J.; Su, H.H.; Xu, J.H.; Zhang, L. Simulation analysis of the influence of dynamic flow stress behavior on chip formation. *Int. J. Adv. Manuf. Technol.* **2018**, *95*, 2301–2313. [\[CrossRef\]](#)
15. Arrazola, P.J.; Aristimuno, P.; Soler, D.; Childs, T. Metal cutting experiments and modelling for improved determination of chip/tool contact temperature by infrared thermography. *CIRP Ann.* **2015**, *64*, 57–60. [\[CrossRef\]](#)
16. Wang, Q.Q.; Liu, Z.Q.; Yang, D.; Mohsan, A.U.H. Metallurgical-based prediction of stress-temperature induced rapid heating and cooling phase transformations for high speed machining Ti-6Al-4V alloy. *Mater. Des.* **2017**, *119*, 208–218. [\[CrossRef\]](#)
17. Song, X.H.; Li, A.H.; Lv, M.H.; Lv, H.J.; Zhao, J. Finite element simulation study on pre-stress multi-step cutting of ti-6al-4v titanium alloy. *Int. J. Adv. Manuf. Technol.* **2019**, *104*, 2761–2771. [\[CrossRef\]](#)
18. Yang, J.H.; Sun, S.J.; Brandt, M.; Yan, W.Y. Experimental investigation and 3D finite element prediction of the heat affected zone during laser assisted machining of Ti6Al4V alloy. *J. Mater. Process. Technol.* **2010**, *210*, 2215–2222. [\[CrossRef\]](#)
19. Wang, L.J.; Zhao, J.; Tan, Q.C. Kinematics of ultrasonic vibration turning and its surface quality. *Acta Armamentarii* **1987**, *3*, 24–31.
20. Ginting, A.; Nouari, M. Surface integrity of dry machined titanium alloys. *Int. J. Mach. Tools Manuf.* **2009**, *49*, 325–332. [\[CrossRef\]](#)
21. Che-Haron, C.H.; Jawaid, A. The effect of machining on surface integrity of titanium alloy Ti-6%Al-4%V. *J. Mater. Process. Technol.* **2005**, *166*, 188–192. [\[CrossRef\]](#)

-
22. Hou, G.M.; Li, A.H.; Song, X.H.; Sun, H.; Zhao, J. Effect of cutting parameters on surface quality in multi-step turning of Ti-6Al-4V titanium alloy. *Int. J. Adv. Manuf. Technol.* **2018**, *5*, 1355–1365. [[CrossRef](#)]
 23. Jiang, A.L.; Zhang, P.Z.; Huang, J. Microstructure and tribological properties of Zr permeating layer on TC11 titanium alloy surface. *Mater. Mech. Eng.* **2011**, *35*, 14–17. [[CrossRef](#)]
 24. Liu, Y.J.; Cheng, K.Q. *Wear Failure Analysis*; Mechanical Industry Press: Beijing, China, 1991.